Energy-valley-dependent charge transfer in few-layer transition metal dichalcogenide heterostructures

Pavel Valencia-Acuna, Stephanie Amos, Hartwin Peelaers,* and Hui Zhao†
Department of Physics and Astronomy, The University of Kansas, Lawrence, Kansas 66045, United States

(Received 13 May 2023; revised 21 July 2023; accepted 24 July 2023; published 7 August 2023)

The effect of the energy valley on interlayer charge transfer in transition metal dichalcogenide (TMD) heterostructures is studied by transient absorption spectroscopy and density functional theory. First-principles calculations confirm that the Λ_{min} valley in the conduction band of few-layer WSe_2 evolves from above its K valley in the monolayer (1L) to below it in 4L. Heterostructure samples of nL-WSe_2/1L-MoS_2, where $n = 1, 2, 3$, and 4, are obtained by mechanical exfoliation and dry transfer. Photoluminescence spectroscopy reveals a thickness-dependent WSe_2 band structure and efficient interlayer charge transfer. Transient absorption measurements show that the electron transfer time from the Λ_{min} valley of 4L WSe_2 to the K valley of MoS_2 is on the order of 30 ps. This process is much slower than the K-K charge transfer in 1L/1L TMD heterostructures. The momentum-indirect interlayer excitons formed after charge transfer have lifetimes >1 ns.

DOI: 10.1103/PhysRevB.108.085302

I. INTRODUCTION

The discovery of graphene [1] has created an exciting research field of two-dimensional (2D) materials, such as transition metal dichalcogenides (TMDs), hexagonal boron nitride, and phosphorene [2,3]. These atomically thin materials possess various features that are attractive to both fundamental research and device applications [4,5]. Moreover, they provide a method to fabricate heterostructures by stacking different types of 2D materials on top of each other [6]. Since the van der Waals interlayer coupling does not require lattice matching, this approach allows arbitrary combination of materials and could produce many artificial materials [7,8].

Interlayer charge transfer plays a key role in harnessing emergent electronic and optical properties of the van der Waals heterostructures. This process has been studied in various 2D heterostructures by using time-resolved techniques including transient absorption [9–16], photoemission, [17] terahertz spectroscopy [18], 2D electronic spectroscopy [19], and second-harmonic generation [20], as well as steady-state optical spectroscopy measurements such as photoluminescence (PL) quenching and absorption line broadening [21–23]. These studies revealed that charge transfer occurs on a time scale <100 fs in many heterostructures with type-II band alignments, where the global conduction band minimum (CBM) and valence band maximum (VBM) are in different materials. Further studies showed that such highly efficient charge transfer is robust with respect to interlayer twist angle [13,21,24–26], lattice temperature [27], dielectric environment [27], carrier density [18], and carrier excess energy [18].

Building on these extensive experimental efforts, significant progress has been made in developing theoretical understanding of the physical mechanisms of interlayer charge transfer. For example, delocalization in momentum space due to strong localization in real space could help articulate the in-plane momentum mismatch [28]. Density functional theory (DFT) has showed that coherent charge oscillations driven by phonons could enable charge transfer [29–31]. The effect of layer-hybridized states on charge transfer has been proposed [30,32] and experimentally confirmed [33]. However, a full understanding of charge transfer mechanisms has not yet been established. Experiments that reveal aspects of charge transfer are highly desirable for such efforts. Previous studies on charge transfer in TMD heterostructures have focused on those between the K valleys of both layers. The effect of the energy valley on charge transfer is largely unexplored.

Here, we show that heterostructures formed by few-layer (nL) and monolayer (1L) TMDs offer a platform to study energy-valley-dependent charge transfer, taking advantage of their thickness-tunable band structures. In the previously studied 1L/1L TMD heterostructures, the carriers are excited in and transfer between the K valleys of the two 1Ls. Using nL-WSe_2/1L-MoS_2 heterostructures as an example, we show that, in contrast to the sub-100-fs K-K transfer, the electron transfer from the Λ_{min} valley of few-layer WSe_2 to the K valley of 1L-MoS_2 can take several tens of picoseconds. These results provide elements to understand interlayer charge transfer and offer a mechanism to design heterostructures with tunable interlayer charge transfer properties.

II. HETEROSTRUCTURE DESIGN AND BAND ALIGNMENT CALCULATION

Figure 1 schematically illustrates the design that enables the study of the energy-valley-dependent charge transfer. It

*peelaers@ku.edu
†huizhao@ku.edu

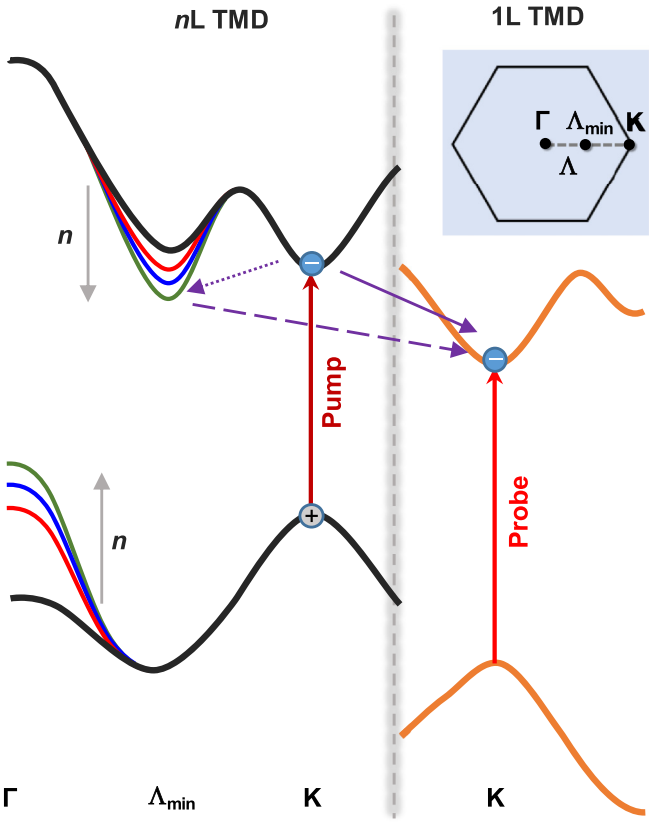

FIG. 1. Schematics of band structures of heterostructures formed by nL and 1L transition metal dichalcogenides (TMDs). The inset shows the involved high-symmetry points in reciprocal space.

has been well established that most TMD 1Ls are direct band gap semiconductors with the CBM and VBM in the K valley. Two TMD 1Ls usually form a type-II heterostructure with layer-separated CBM and VBM (black and orange curves). Previous DFT calculations (see, for example, Refs. [34,35]) indicated that, in most TMDs, the $\Lambda_{\min}$ valley of the conduction band drops with thickness. Here, $\Lambda_{\min}$ is a point on the Λ high-symmetry line (which connects the Γ and K points) where the energy is minimal. If the $\Lambda_{\min}$ valley of the few-layer TMD is comparable with or below its K valley (while still being above the K valley of the other TMD), electrons photoexcited in the K valley could be scattered to the $\Lambda_{\min}$ valley (dotted purple arrow). Previous studies have shown that the intervalley scattering times in 1L, few-layer, and bulk TMDs are on the order of 100 fs [36–39]. Hence, although this process competes with (and is less efficient than) the interlayer charge transfer between the two K valleys (solid purple arrow), a fraction of the electron population could temporarily populate this valley. These electrons could undergo a $\Lambda_{\min}$-K interlayer transfer (dashed purple arrow) as their only relaxation pathway, offering an opportunity to study interlayer transfer of electrons between different energy valleys.

We use DFT to reveal the thickness-tunable band structure of such heterostructures, using nL-WSe_2/1L-MoS_2 as an example. All calculations are performed using VASP [40,41] with projector augmented-wave [42] potentials. Given the layered nature of the materials, van der Waals forces are explicitly

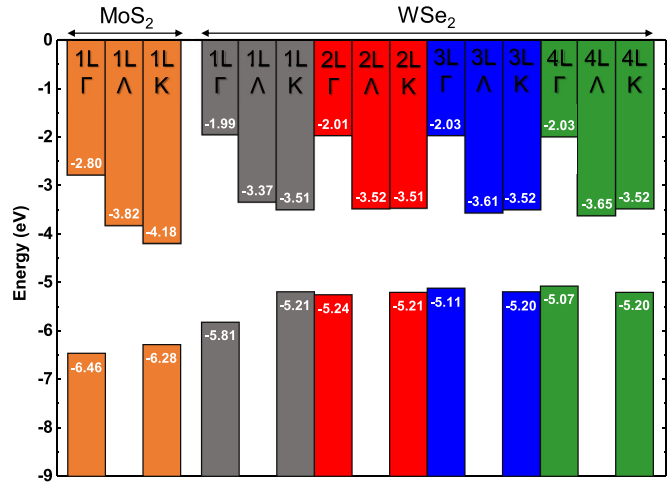

FIG. 2. Calculated band alignments with respect to the vacuum level for, from left to right: 1L-MoS_2, 1L-WSe_2, 2L-WSe_2, 3L-WSe_2, and 4L-WSe_2.

included using the Grimme DFT-D2 method [43,44]. To obtain accurate band gaps and alignments, we use the HSE06 hybrid functional [45,46]. Spin-orbit coupling is included. An energy cutoff of 300 eV is used for the plane-wave basis, and all structures are fully relaxed so that the maximum force is <5 meV/Å. The layers are separated by at least 11.7 Å of vacuum. All band structures are aligned to the vacuum level. An explicit heterostructure calculation is performed to ensure that the alignments obtained using separate TMD calculations remain valid in the heterostructures.

Figure 2 summarizes the DFT results. The calculated band gap of 1L-MoS_2 is 2.1 eV and of 1L-WSe_2 is 1.7 eV. The K valley of WSe_2 remains at -3.5 eV below the vacuum level, independent of the number of layers, as these states are mainly from the d orbitals of the W atoms. The $\Lambda_{\min}$ valley decreases from -3.4 eV in 1L to -3.6 eV in 4L due to the contributions from the p orbitals of the Se atoms. Hence, with increasing n, the $\Lambda_{\min}$ valley of WSe_2 evolves from being a few times of k_BT above its K valley to a few times of k_BT below it, where k_BT is the lattice thermal energy at room temperature (26 meV). This feature is qualitatively consistent with a recent study [35]. With the K valley of 1L-MoS_2 at -4.2 eV, the heterostructures remain type II. Hence, these heterostructures offer an ideal platform to study the energy-valley-dependent charge transfer. We note that these calculations on individual materials do not include layer hybridization, which could alter the energy of some of these valleys in the heterostructures. However, our results provide a good starting point to understand these heterostructures.

III. SAMPLE FABRICATION AND CHARACTERIZATION

The heterostructure sample is fabricated by exfoliation and dry transfer techniques. Flakes of WSe_2 and MoS_2 are exfoliated from their bulk crystals by pressing and peeling off thermal release tapes and are then transferred to polydimethylsiloxane (PDMS) substrates. A WSe_2 thin flake with regions of various thickness is selected and transferred onto a SiO_2/Si substrate, as shown in Fig. 3. Optical contrasts of

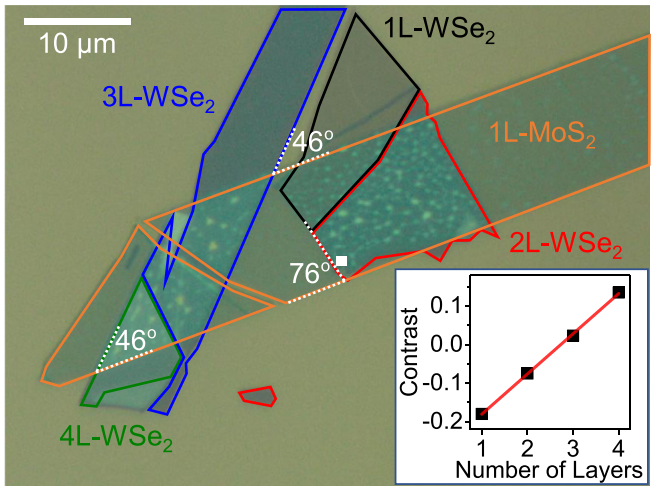

FIG. 3. Optical microscope image of the nL-WSe_2/1L-MoS_2 heterostructure sample. The inset shows the contrast of different regions of the WSe_2 flake plotted against the assigned number of layers.

different regions are analyzed and plotted in the inset against the assigned number of layers. The contrast is defined as the difference in the green-channel counts between the flake and bare PDMS substrate, divided by the latter. A clear steplike feature of the contrast is observed. Since the contrast is proportional to the thickness of such a thin film on a thick and transparent substrate, we can safely assign the layer numbers accordingly. Next, a 1L-MoS_2 flake, which is exfoliated with the same procedure, is transferred onto the WSe_2 flake. The angles between the long edges of the $MoSe_2$ and WSe_2 flakes, which are along their high-symmetry directions, are labeled in Fig. 3. These large twist angles ensure that the samples are not aligned heterostructures (0° or 60°), which could have very different interlayer interactions from the randomly stacked ones, since our goal is to study the thickness dependence. The sample is thermally annealed at 200 °C in Ar atmosphere for 4 h.

PL spectroscopy is performed under a continuous-wave laser excitation of 1.96 eV and 1 μW, with a spot size of ∼2 μm [47]. Figure 4 shows the results. The peaks at 1.90 (orange curve in the top panel) and 1.65 eV (pink curve in the top panel) from the 1L-MoS_2 and 1L-WSe_2 regions, respectively, are consistent with previous reports [47,48]. They originate from the excitons with both electrons and holes in the K valley (labeled as K-K transition). The DFT calculation shows higher energies (2.10 and 1.70 eV, respectively) than the PL peaks. Two factors could contribute to the discrepancy. First, the exciton binding energies (the difference between the band gap and the exciton energy) in 2D semiconductors are as large as several hundreds of millielectronvolts [49,50]. Second, DFT often overestimates the band gap of 2D materials due to the approximations made in the exchange-correlation functional [51]. In 2L-WSe_2, the PL peak redshifts, and its yield decreases by a factor of 15, indicating the impact of its indirect band gap. We attribute this broad peak centered at ∼1.60 eV to the excitons with electrons in the Λ_{min} or K valleys and holes in the Γ or K valleys, according to our DFT

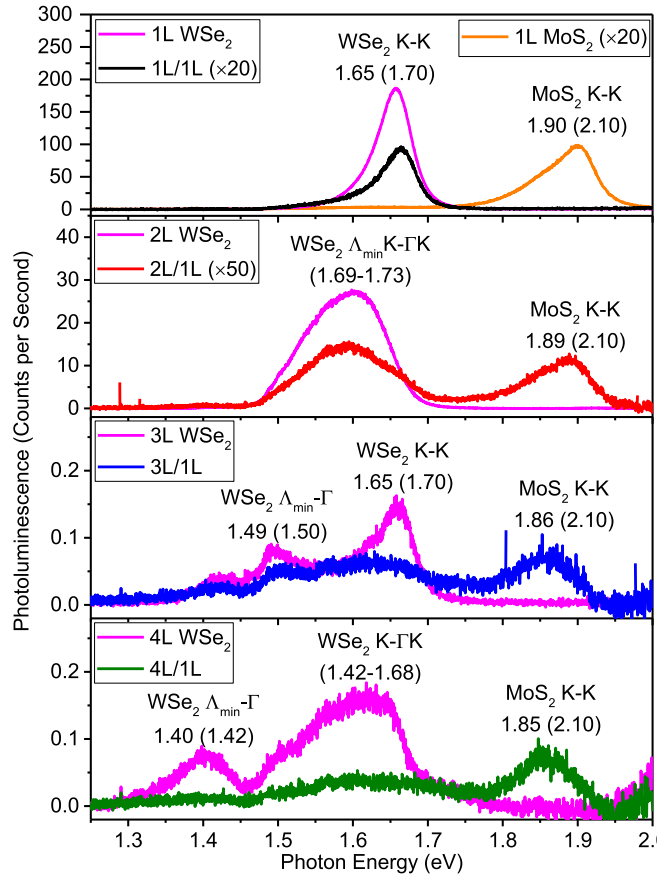

FIG. 4. Photoluminescence spectra of the heterostructures and their individual materials. Pink curves are from WSe_2 flakes with increasing layer number (top to bottom), while the orange curve is from 1L-MoS_2. The results from four heterostructures are shown as the black, red, blue, and green curves. Some spectra are scaled for clarity, with scaling factors indicated in the legends. Peaks are assigned to various transitions with the format of conduction band valley(s)–valence band valley(s). The numbers indicate the observed peak positions in eV. The numbers in parentheses are the corresponding interband transition energy (in eV) according to our density functional theory (DFT) results (Fig. 2).

results (Fig. 2). In 3L-WSe_2, the PL yield drops by two orders of magnitude from 2L, with the reappearance of a 1.65-eV K-K peak and a redshifted Λ_{min}-Γ peak at 1.49 eV. The latter further shifts to 1.40 eV in 4L WSe_2. We attribute the broad feature at 1.60 eV from the 4L sample to the excitons with electrons in K and holes in Γ or K valleys. These results are very consistent with previous results on thickness-dependent PL from WSe_2 [48] and are reasonably reproduced in our DFT calculations, despite the discrepancy in the absolute numbers as discussed above.

The PL spectra from the four heterostructure samples are measured under the same excitation conditions as the individual materials discussed above. In the 1L/1L heterostructure (black, top panel), the WSe_2 peak is quenched by ∼40 times compared with 1L-WSe_2. Such a significant quenching indicates that efficient electron transfer from WSe_2 to MoS_2 occurs on a time scale much shorter than the recombination lifetime of the excitons in WSe_2 [21–23]. In the 2L/1L

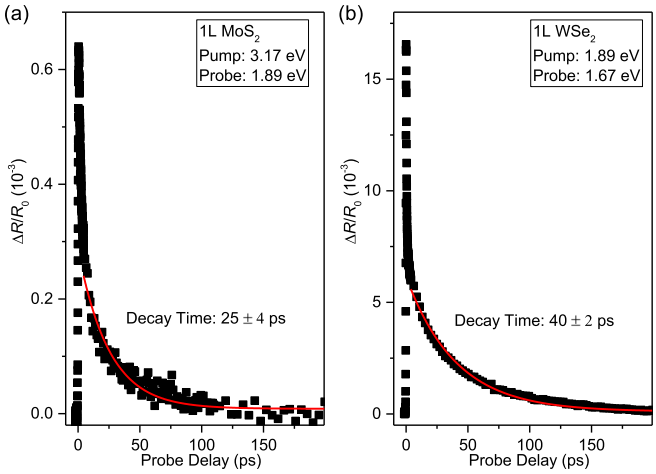

FIG. 5. Differential reflectance of (a) 1L-MoS2$_2$ and (b) 1L-WSe_2 with pump and probe photon energies as labeled. The red curves are exponential fits.

heterostructure, the 2L-WSe_2 peak is quenched by ∼100 times (red), while in the 3L/1L and 4L/1L heterostructures, the WSe_2 PL is only moderately quenched since the PLs from 3L- and 4L-WSe_2 are rather weak. The MoS_2 peak in the heterostructures is quenched by ∼20–100 times, indicating efficient hole transfer from MoS_2 to WSe_2. Furthermore, this peak redshifts as the thickness of WSe_2 is increased. Previously, the redshift of the PL peak of 1L-TMD in 1L/1L heterostructures has been well observed and attributed to the screening effect [52]. Our observation is consistent with this interpretation since a large screening effect is expected with thicker WSe_2 layers. No PL peaks from interlayer excitons (IXs) are observed in this spectral range since they are expected to be at ∼1 eV, according to our DFT results (Fig. 2).

The 1L samples are further characterized by transient absorption measurements in reflection geometry. The homemade setup is based on a mode-locked Ti-doped sapphire laser (80 MHz), an optical parametric oscillator, and second-harmonic generation units. The details of the setup were described previously [47]. Figure 5(a) shows the result of the 1L-MoS_2 with pump and probe photon energies of 3.17 and 1.89 eV, respectively. The 3.17-eV pump pulse with a peak fluence of 0.1 μJ cm^{-2} injects electron-hole pairs by interband absorption. The 1.89-eV probe monitors the dynamics of the injected carriers by its differential reflectance, which is defined as $\Delta R/R_0 = (R - R_0)/R_0$, where R and R_0 are the reflectance with and without the pump pulse, respectively. After a few-picosecond fast delay, which is due to the exciton formation process [53,54], the long-term decay of the signal can be fit by an exponential function (red curve). The decay time constant of 25 ps is assigned to the exciton lifetime in 1L-MoS_2. Similarly, Fig. 5(b) shows the results of 1L-WSe_2 with 0.5 μJ cm^{-2} and 1.89-eV pump and 1.67-eV probe pulses. The deduced exciton lifetime is ∼40 ps.

IV. INTERLAYER CHARGE TRANSFER

Transient absorption measurements are performed to study the interlayer charge transfer process in the nL-WSe_2/1L-MoS_2 heterostructure samples. Here, a 1.67-eV pump pulse is used to excite the K valley of WSe_2, as schematically shown in Fig. 1. With a peak energy fluence of 1 μJ cm^{-2}, the pump injects a peak carrier density of 3.8×10^{11} cm^{-2} in each WSe_2 layer, which is estimated by using a monolayer absorbance of 0.04 [55]. At this density, the average distance between the carriers is ∼16 nm. In such a low-density regime, the effect of carrier interaction on their dynamics can be ignored, and the differential reflectance is proportional to the carrier density. The 1.89-eV probe, with a fluence of ∼0.2 μJ cm^{-2}, is tuned to the optical band gap of 1L-MoS_2 (Fig. 1) to effectively probe the carriers in the MoS_2 layer [56]. Figure 6 summarizes the key results of the transient absorption measurements, which reveal various types of carrier dynamics as illustrated in Fig. 6(a), including the K-K electron transfer [solid purple arrow, (i)], the K-Λ_{min} intervalley scattering (dotted purple arrow), the Λ_{min}-K electron transfer [dashed purple arrow, (ii)], and the Γ-K IX recombination [red double arrow, (iii)]. Figures 6(b)–6(d) show the differential reflectance signals obtained from all the sample regions in short, intermediate, and long time ranges, revealing the processes labeled as (i)–(iii), respectively.

Although the 1.89-eV probe is intended to detect carriers in MoS_2, a signal is observed from the 1L-WSe_2 region of the sample, as shown as the open squares in Figs. 6(b) and 6(d). Since the probe photon energy is above the optical band gap of WSe_2 of 1.67 eV, the signal is due to the reflectance change at higher energy states of WSe_2 due to the pump-injected excitons. The rise of the signal can be fit by the integral of a Gaussian function with a full width at half maximum (FWHM) of 0.46 ps [solid gray curve in Fig. 6(b)], which is close to the expected instrument response time with the pump and probe pulse widths of ∼0.3 ps. The decay of the signal can be fit by an exponential function with a decay time of 44 ± 2 ps, as indicated by the gray curve in Fig. 6(d). This result agrees well with that shown in Fig. 5(b) (which was obtained by the more conventional pump/probe configuration of 1.89 eV/1.67 eV) and previous differential reflectance measurements of 1L-WSe_2 [57]. Hence, although the probe photon energy here is higher than the pump, it still probes carriers in WSe_2 effectively. When the measurement is performed on the 1L-MoS_2 region, however, no signal is observed [orange circles in Figs. 6(b) and 6(d)], showing that the 1.67-eV pump does not excite carriers in MoS_2. Otherwise, a signal like that shown in Fig. 5(a) would have been observed.

Next, we discuss the results from the heterostructure regions. We start with the signal from the 1L/1L heterostructure, as shown by the solid black squares in Fig. 6(b). Two processes contribute to the rise of the signal: First, the electrons excited in WSe_2 can transfer to MoS_2, producing a strong signal as the probe is tuned to the MoS_2 optical band gap. This transfer process can be described by $N(t) = N_0[1 - \exp(-t/\tau_t)]$, where N and N_0 are the time-dependent electron density in MoS_2 and the total density of the electrons participating the transfer process, respectively, while τ_t is the charge transfer time. Second, the holes excited in (and remain in) WSe_2 immediately produce a signal since the probe is also coupled to the high-energy states of WSe_2, as is observed in the 1L-WSe_2 region (open squares). However, we find that the

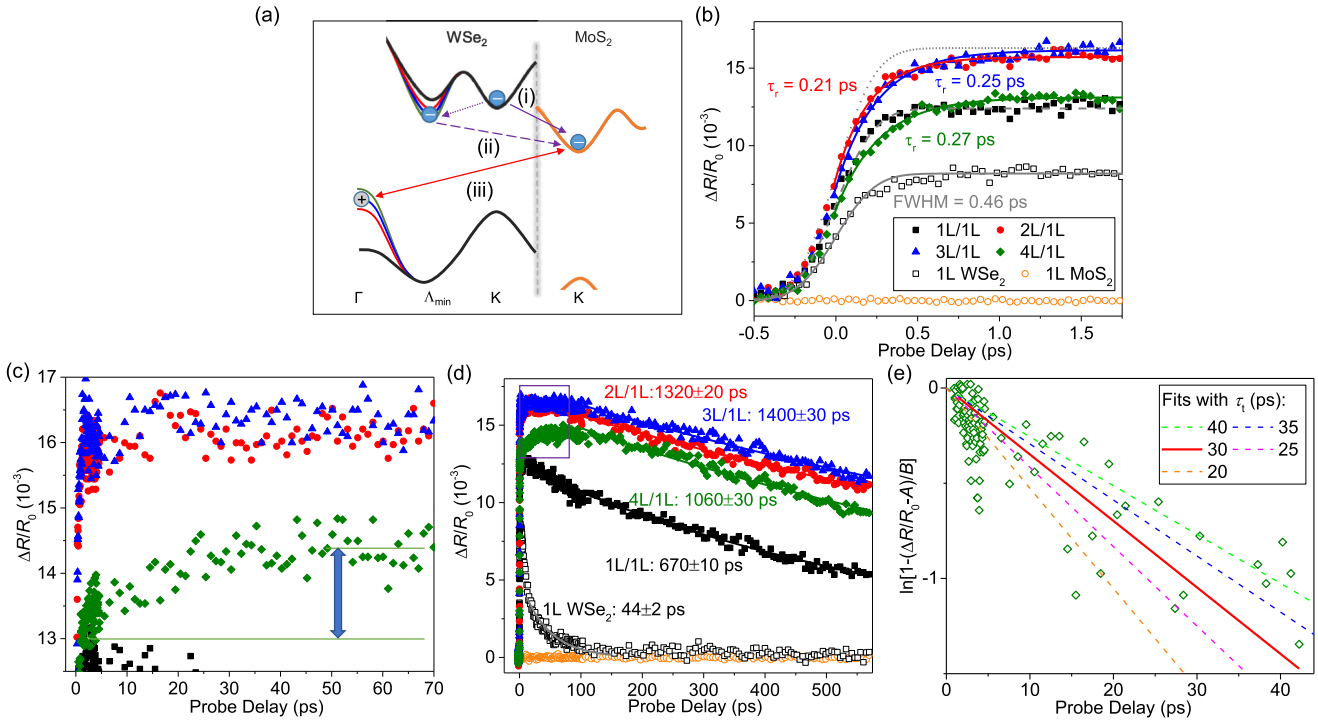

FIG. 6. (a) Schematics of the photocarrier dynamics. (b) Differential reflectance measured from different samples for a short time range. The samples are excited with a 1.67-eV pump pulse and probe with a 1.89-eV pulse. Solid symbols are from heterostructure samples of 1L/1L (black squares), 2L/1L (red circles), 3L/1L (blue triangles), and 4L/1L (green diamonds), while open symbols represent results from 1Ls of WSe_2 (gray squares) and MoS_2 (orange circles). The gray curves represent the instrument response function. The red, blue, and green curves are fits with the charge transfer model. They reveal the K-K charge transfer as indicated by the solid purple arrow. (c) Same as (b) but over a longer time range. The slow rise of the signal in the 4L/1L sample reveals the Λ_{min}-K charge transfer [dashed purple arrow in (a)]. (d) Same as (b) but over the full range of time. The box indicates the range shown in (c). The curves are exponential fits to the decay. They reveal recombination of the Γ-K interlayer excitons. (e) Analysis of the slow-rising component. Open symbols are calculated from the data shown in (c). Lines are fits with different charge transfer times.

rise of this signal matches the Gaussian integral of FWHM = 0.46 ps [dashed gray curve in Fig. 6(b)] that represents the instrument response time, while the magnitude of the signal is larger than that of 1L-WSe_2. The increased signal magnitude shows that most electrons excited in WSe_2 transferred to MoS_2 since, without the electron population in MoS_2, the signal from the heterostructure would have been of similar magnitude to 1L-WSe_2. The instrument-limited rise time thus indicates that the transfer occurs on a time scale shorter than the instrument response time, which is consistent with both previous studies on 1L/1L-TMD heterostructures [9–16] and the significant PL quenching discussed above (Fig. 4). Hence, this feature confirms the ultrafast K-K electron transfer process in the 1L/1L heterostructure [the solid purple arrow in Fig. 6(a)]. We note that, after the rise, the signal from the heterostructure (at 1 ps) is $\sim 12 \times 10^{-3}$, with an expected contribution from the holes in WSe_2 of $\sim 3.5 \times 10^{-3}$ [which is half of the signal from 1L-WSe_2, open squares in Fig. 6(b), assuming electrons and holes make equal contribution to the signal in 1L-WSe_2].

Increasing the layer number of WSe_2, the rise of the signal slows down. To better illustrate this trend, the dotted gray curve in Fig. 6(b) indicates the instrument-limited 0.46-ps Gaussian integral, which is scaled to match the peak of the signals. Clearly, the signal rise is no longer limited by the instrument response. Instead, the rise of the signals from 2L/1L, 3L/1L, and 4L/1L heterostructures can be fit by the aforementioned charge-transfer model with transfer times of 0.21, 0.25, and 0.27 ps, respectively. We attribute these time constants to the K-K electron transfer time. We thus confirm that the K-K electron transfer from few-layer WSe_2 to 1L-MoS_2 remains ultrafast. The slight increase of the transfer time with the layer number of WSe_2 could be attributed to the additional transfer process of the electrons between different WSe_2 layers toward MoS_2.

Figure 6(c) shows the differential reflectance signals on the intermediate time scale of up to 70 ps. Interestingly, after the initial fast rise, a relatively slow-rising component of the signal emerges in the 4L/1L heterostructure (green diamonds), which is absent in all other samples. Based on the band alignment shown in Fig. 2, we propose the following carrier dynamics: In the 1L/1L heterostructure, the K-K electron transfer is the dominant channel for the excited electrons, which occurs on an ultrafast time scale. In 4L-WSe_2, however, the Λ_{min} valley is 130 meV lower than its K valley, according to our DFT results. Hence, some of the electrons excited to the K valley can scatter to the Λ_{min} valley as a competing process to their transfer to MoS_2. Once scattered, these electrons can only transfer to the K valley of MoS_2 since their backscattering to the K valley of WSe_2 is energy unfavorable. This Λ_{min}-K charge transfer produces the slow-rising signal. We note that the K-K

transfer of electrons in different layers of WSe_2 makes minimal contribution on this time scale since most electrons populate the Λ_{min}.

To quantify this transfer process, we note that the rise of the signal due to the Λ_{min}-K charge transfer can be written as $\Delta R/R_0 = A + B[1 - \exp(-t/\tau_t)]$, where A represents the background signal at $t = 0$ that is not associated with the transfer process, and B is the peak signal produced after all electrons have transferred. To better extract the transfer time and probe its uncertainty, we convert this equation to $\ln[1 - (\Delta R/R_0 - A)/B] = -t/\tau_t$. The calculated $\ln[1 - (\Delta R/R_0 - A)/B]$ from the data is plotted in Fig. 6(e). By a linear fit (solid red line), we deduce a charge transfer time of ∼30 ps. The dashed lines correspond to this model with different transfer times, which confirm that the uncertainty of the transfer time is at most ±10 ps. Furthermore, this slow-rising component is ∼20% of the fast-rising component. This suggests that the number of the excited electrons following the fast K-K transfer channel is a few times more than those scattered to the Λ_{min} valley, which is consistent with previous results on the intervalley scattering [36–39] and charge transfer times [9–17].

The 2L- and 3L-WSe_2 heterostructures represent intermediate systems, where the slow-rising component is insignificant. In 2L-WSe_2, the Λ_{min} valley is nearly degenerate with the K valley. Hence, although some of the excited electrons can be scattering to the Λ_{min} valley as a competing process to their transfer to MoS_2, they can scatter back to the K valley, allowing their fast transfer to MoS_2 by the K-K process. The slow-rising component is not observed in the 3L/1L heterostructure, while the Λ_{min} valley is predicted to be 90 meV below the K valley (Fig. 2). This could be attributed to potential backscattering of electrons to the K valley or overestimation of the energy difference by the calculation. We note that the magnitude of the signals from different heterostructures may not accurately reflect the transferred electron density due to two factors. First, the signal is sensitive to the interfacial quality since parts of a sample with poor interface would not contribute to the signal. Second, the MoS_2 exciton resonance shifts with WSe_2 thickness, as shown in Fig. 4. This can cause different amounts of detuning between the probe (1.89 eV) and the exciton resonances in different samples.

To speculate possible origins of the slow Λ_{min}-K charge transfer, we first address the issue of the twist angle. In general, the twist angle between the two layers can have profound effect on the properties of IXs, such as their energy states [58], recombination [59], interlayer hybridization [33], and valley polarization [60]. With certain twist angles, moiré patterns can form, which can tune the in-plane properties of the IXs [61–63]. However, several studies have shown that the twist angle has minimal effect on the K-K interlayer charge transfer time. For example, one study found that the charge transfer time is <40 fs in a large number of MoS_2/WSe_2 heterostructure samples with various twist angles [13]. In another study, the charge-transfer-induced PL quenching was found to be consistent across >20 WS_2/WSe_2 heterostructures with random twist angles [25]. A charge transfer time of ∼90 fs is observed in 12 randomly twisted MoS_2/WS_2 samples. [26]. These results are consistent with the fact that ultrafast charge transfer has been generally observed by different groups from different samples with random and often unknown twist angles [9–20]. Moreover, a recent theoretical study showed that the twist angle has weak influence on charge transfer time, even though it strongly influences the IX recombination, in MoS_2/WS_2 heterostructures [64]. All the heterostructures studied here have large twist angles and are in the weakly coupled regime. Hence, we do not expect the large difference in charge transfer times observed is due to the uncertainties on twist angle. As another factor, the electron transfer is driven by the conduction band offset, which decreases with thickness, as shown in Fig. 1. This could result in a thickness-dependent transfer time. However, the band offset in the 4L/1L heterostructure is 620 meV, which is much larger than most other types of TMD heterostructures, where ultrafast K-K charge transfer has been generally observed [9–20]. Finally, the space-charge field induced by the transferred carriers is unlikely to be responsible for the observed effect because, with the injected carrier densities used in this study, it only produces a potential energy difference on the order of 10 meV [18,65], much smaller than the band offsets of all heterostructures studied here. Hence, further theoretical efforts are needed to understand the physics mechanism of the slow Λ_{min}-K charge transfer.

Figure 6(d) shows the long-term decay of the signals, which can be fit by single-exponential functions with decay times as labeled. The decay of the signal monitors the lifetime of the electrons in the K valley of MoS_2. Since the K valley is the lowest conduction band energy valley in MoS_2, the decay of the electron population is mainly due to their recombination with the holes in WSe_2. Hence, the decay times reflect the recombination lifetimes of the IXs. For the 1L/1L heterostructure, the IXs are formed by the K-valley electrons in MoS_2 and the K-valley holes in WSe_2. They have a lifetime of 670 ps, which is much longer than the intralayer exciton lifetime of 44 ± 2 ps in 1L-WSe_2 (gray curve). In the other three heterostructures, the holes in WSe_2 reside in the Γ valley, as shown in Fig. 6(a). Hence, the IXs are also indirect in momentum space, or intervalley, in nature. The recombination lifetimes of such Γ-K intervalley IXs are >1 ns. However, we do not understand the variation of the lifetime among these three heterostructures (1060–1400 ps).

V. CONCLUSIONS

We have observed, by interfacing few-layer WSe_2 with 1L-MoS_2, charge transfer between different energy valleys. Due to the crystal momentum mismatch, the electron transfer from the Λ_{min} valley of 4L-WSe_2 to the K valley of 1L-MoS_2 is ∼30 ps, which is about two orders of magnitude slower than the K-K charge transfer that has been previously studied. Extended recombination lifetimes of the momentum-indirect IXs to >1 ns are also observed. These results provide experimental data for understanding the interlayer charge transfer mechanisms, reveal the important role of the energy valley in this process, and offer a method to control the charge transfer rate. Few-layer TMD heterostructures have larger light absorbance than monolayer heterostructures and hence can improve performance of optoelectronic devices. Our results provide basic parameters of such heterostructures.

ACKNOWLEDGMENTS

H.Z. acknowledges support by the U.S. Department of Energy, Office of Basic Energy Sciences, Division of Materials Sciences and Engineering under Award No. DE-SC0020995. H.P. is supported by U.S. National Science Foundation (DMR 2109979). P.V.A. is supported by KU Research GO and GRF. This paper used Bridges-2 at the Pittsburgh Supercomputing Center through allocation DMR200079 from the Advanced Cyberinfrastructure Coordination Ecosystem: Services & Support (ACCESS) program, which is supported by National Science Foundation Grants No. 2138259, No. 2138286, No. 2138307, No. 2137603, and No. 2138296.

[1] K. S. Novoselov, A. K. Geim, S. V. Morozov, D. Jiang, Y. Zhang, S. V. Dubonos, I. V. Grigorieva, and A. A. Firsov, Electric field effect in atomically thin carbon films, Science **306**, 666 (2004).

[2] E. Gibney, The super materials that could trump graphene, Nature (London) **522**, 274 (2015).

[3] A. H. C. Neto and K. Novoselov, New directions in science and technology: Two-dimensional crystals, Rep. Prog. Phys. **74**, 082501 (2011).

[4] Q. H. Wang, K. Kalantar-Zadeh, A. Kis, J. N. Coleman, and M. S. Strano, Electronics and optoelectronics of two-dimensional transition metal dichalcogenides, Nat. Nanotechnol. **7**, 699 (2012).

[5] Z. Lin, A. McCreary, N. Briggs, S. Subramanian, K. H. Zhang, Y. F. Sun, X. F. Li, N. J. Borys, H. T. Yuan, S. K. Fullerton-Shirey *et al.*, 2D materials advances: From large scale synthesis and controlled heterostructures to improved characterization techniques, defects and applications, 2D Mater. **3**, 042001 (2016).

[6] A. K. Geim and I. V. Grigorieva, Van der Waals heterostructures, Nature (London) **499**, 419 (2013).

[7] Y. Liu, N. O. Weiss, X. Duan, H.-C. Cheng, Y. Huang, and X. Duan, Van der Waals heterostructures and devices, Nat. Rev. Mater. **1**, 16042 (2016).

[8] K. S. Novoselov, A. Mishchenko, A. Carvalho, and A. H. C. Neto, 2D materials and van der Waals heterostructures, Science **353**, aac9439 (2016).

[9] X. Hong, J. Kim, S. F. Shi, Y. Zhang, C. Jin, Y. Sun, S. Tongay, J. Wu, Y. Zhang, and F. Wang, Ultrafast charge transfer in atomically thin MoS_2/WS_2 heterostructures, Nat. Nanotechnol. **9**, 682 (2014).

[10] F. Ceballos, M. Z. Bellus, H. Y. Chiu, and H. Zhao, Ultrafast charge separation and indirect exciton formation in a MoS_2-$MoSe_2$ van der Waals heterostructure, ACS Nano **8**, 12717 (2014).

[11] F. Ceballos, M. Z. Bellus, H. Y. Chiu, and H. Zhao, Probing charge transfer excitons in a $MoSe_2$-WS_2 van der Waals heterostructure, Nanoscale **7**, 17523 (2015).

[12] B. Peng, G. Yu, X. Liu, B. Liu, X. Liang, L. Bi, L. Deng, T. C. Sum, and K. P. Loh, Ultrafast charge transfer in MoS_2/WSe_2 *p-n* heterojunction, 2D Mater. **3**, 025020 (2016).

[13] H. M. Zhu, J. Wang, Z. Z. Gong, Y. D. Kim, J. Hone, and X. Y. Zhu, Interfacial charge transfer circumventing momentum mismatch at two-dimensional van der Waals heterojunctions, Nano Lett. **17**, 3591 (2017).

[14] L. Yuan, T. F. Chung, A. Kuc, Y. Wan, Y. Xu, Y. P. Chen, T. Heine, and L. B. Huang, Photocarrier generation from interlayer charge-transfer transitions in WS_2-graphene heterostructures, Sci. Adv. **4**, e1700324 (2018).

[15] X. W. Wen, H. L. Chen, T. M. Wu, Z. H. Yu, Q. R. Yang, J. W. Deng, Z. T. Liu, X. Guo, J. X. Guan, X. Zhang *et al.*, Ultrafast probes of electron-hole transitions between two atomic layers, Nat. Commun. **9**, 1859 (2018).

[16] L. Wu, Y. Chen, H. Zhou, and H. Zhu, Ultrafast energy transfer of both bright and dark excitons in 2D van der Waals heterostructures beyond dipolar coupling, ACS Nano **13**, 2341 (2019).

[17] F. Liu, Q. Y. Li, and X. Y. Zhu, Direct determination of momentum-resolved electron transfer in the photoexcited van der Waals heterobilayer WS_2/MoS_2, Phys. Rev. B **101**, 201405(R) (2020).

[18] E. Y. Ma, B. Guzelturk, G. Q. Li, L. Y. Cao, Z. X. Shen, A. M. Lindenberg, and T. F. Heinz, Recording interfacial currents on the subnanometer length and femtosecond time scale by terahertz emission, Sci. Adv. **5**, eaau0073 (2019).

[19] V. R. Policht, M. Russo, F. Liu, C. Trovatello, M. Maiuri, Y. Bai, X. Zhu, S. D. Conte, and G. Cerullo, Dissecting interlayer hole and electron transfer in transition metal dichalcogenide heterostructures via two-dimensional electronic spectroscopy, Nano Lett. **21**, 4738 (2021).

[20] P. Yao, D. He, P. Zereshki, Y. Wang, and H. Zhao, Nonlinear optical effect of interlayer charge transfer in a van der Waals heterostructure, Appl. Phys. Lett. **115**, 263103 (2019).

[21] A. F. Rigos, H. M. Hill, Y. L. Li, A. Chernikov, and T. F. Heinz, Probing interlayer interactions in transition metal dichalcogenide heterostructures by optical spectroscopy: MoS_2/WS_2 and $MoSe_2/WSe_2$, Nano Lett. **15**, 5033 (2015).

[22] D. Kozawa, A. Carvalho, I. Verzhbitskiy, F. Giustiniano, Y. Miyauchi, S. Mouri, A. H. C. Neto, K. Matsuda, and G. Eda, Evidence for fast interlayer energy transfer in $MoSe_2/WS_2$ heterostructures, Nano Lett. **16**, 4087 (2016).

[23] B. W. Yang, E. Molina, J. Kim, D. Barroso, M. Lohmann, Y. W. Liu, Y. D. Xu, R. Q. Wu, L. Bartels, K. Watanabe *et al.*, Effect of distance on photoluminescence quenching and proximity-induced spin-orbit coupling in graphene/WS_2 heterostructures, Nano Lett. **18**, 3580 (2018).

[24] J. R. Schaibley, P. Rivera, H. Y. Yu, K. L. Seyler, J. Q. Yan, D. G. Mandrus, T. Taniguchi, K. Watanabe, W. Yao, and X. D. Xu, Directional interlayer spin-valley transfer in two-dimensional heterostructures, Nat. Commun. **7**, 13747 (2016).

[25] K. Wang, B. Huang, M. Tian, F. Ceballos, M.-W. Lin, M. Mahjouri-Samani, A. Boulesbaa, A. A. Puretzky, C. M. Rouleau, M. Yoon *et al.*, Interlayer coupling in twisted WSe_2/WS_2 bilayer heterostructures revealed by optical spectroscopy, ACS Nano **10**, 6612 (2016).

[26] Z. H. Ji, H. Hong, J. Zhang, Q. Zhang, W. Huang, T. Cao, R. X. Qiao, C. Liu, J. Liang, C. H. Jin *et al.*, Robust

stacking-independent ultrafast charge transfer in MoS_2/WS_2 bilayers, ACS Nano **11**, 12020 (2017).
[27] H. Z. Zhou, Y. D. Zhao, and H. M. Zhu, Dielectric environment-robust ultrafast charge transfer between two atomic layers, J. Phys. Chem. Lett. **10**, 150 (2019).
[28] X. Zhu, N. R. Monahan, Z. Gong, H. Zhu, K. W. Williams, and C. A. Nelson, Charge transfer excitons at van der Waals interfaces, J. Am. Chem. Soc. **137**, 8313 (2015).
[29] H. Wang, J. Bang, Y. Y. Sun, L. B. Liang, D. West, V. Meunier, and S. B. Zhang, The role of collective motion in the ultrafast charge transfer in van der Waals heterostructures, Nat. Commun. **7**, 11504 (2016).
[30] Q. J. Zheng, W. A. Saidi, Y. Xie, Z. G. Lan, O. V. Prezhdo, H. Petek, and J. Zhao, Phonon-assisted ultrafast charge transfer at van der Waals heterostructure interface, Nano Lett. **17**, 6435 (2017).
[31] R. Long and O. V. Prezhdo, Quantum coherence facilitates efficient charge separation at a $MoS_2/MoSe_2$ van der Waals junction, Nano Lett. **16**, 1996 (2016).
[32] Y. Wang, Z. Wang, W. Yao, G. B. Liu, and H. Y. Yu, Interlayer coupling in commensurate and incommensurate bilayer structures of transition-metal dichalcogenides, Phys. Rev. B **95**, 115429 (2017).
[33] N. R. Wilson, P. V. Nguyen, K. Seyler, P. Rivera, A. J. Marsden, Z. P. L. Laker, G. C. Constantinescu, V. Kandyba, A. Barinov, N. D. M. Hine *et al.*, Determination of band offsets, hybridization, and exciton binding in 2D semiconductor heterostructures, Sci. Adv. **3**, e1601832 (2017).
[34] J. E. Padilha, H. Peelaers, A. Janotti, and C. G. Van de Walle, Nature and evolution of the band-edge states in MoS_2: From monolayer to bulk, Phys. Rev. B **90**, 205420 (2014).
[35] H. G. Kim and H. J. Choi, Thickness dependence of work function, ionization energy, and electron affinity of Mo and W dichalcogenides from DFT and GW calculations, Phys. Rev. B **103**, 085404 (2021).
[36] K. Kaasbjerg, K. S. Thygesen, and K. W. Jacobsen, Phonon-limited mobility in *n*-type single-layer MoS_2 from first principles, Phys. Rev. B **85**, 115317 (2012).
[37] N. Kumar, J. He, D. He, Y. Wang, and H. Zhao, Charge carrier dynamics in bulk MoS_2 crystal studied by transient absorption microscopy, J. Appl. Phys. **113**, 133702 (2013).
[38] R. Wallauer, J. Reimann, N. Armbrust, J. Güdde, and U. Höfer, Intervalley scattering in MoS_2 imaged by two-photon photoemission with a high-harmonic probe, Appl. Phys. Lett. **109**, 162102 (2016).
[39] Z. G. Nie, R. Long, J. S. Teguh, C. C. Huang, D. W. Hewak, E. K. L. Yeow, Z. X. Shen, O. V. Prezhdo, and Z. H. Loh, Ultrafast electron and hole relaxation pathways in few-layer MoS_2, J. Phys. Chem. C **119**, 20698 (2015).
[40] G. Kresse and J. Hafner, *Ab initio* molecular dynamics for liquid metals, Phys. Rev. B **47**, 558 (1993).
[41] G. Kresse and J. Furthmüller, Efficient iterative schemes for *ab initio* total-energy calculations using a plane-wave basis set, Phys. Rev. B **54**, 11169 (1996).
[42] P. E. Blöchl, Projector augmented-wave method, Phys. Rev. B **50**, 17953 (1994).
[43] S. Grimme, Semiempirical GGA-type density functional constructed with a long-range dispersion correction, J. Comput. Chem. **27**, 1787 (2006).
[44] H. Peelaers and C. G. Van de Walle, First-principles study of van der Waals interactions in MoS_2 and MoO_3, J. Phys.: Condens. Matter **26**, 305502 (2014).
[45] J. Heyd, G. E. Scuseria, and M. Ernzerhof, Hybrid functionals based on a screened Coulomb potential, J. Chem. Phys. **118**, 8207 (2003).
[46] J. Heyd, G. E. Scuseria, and M. Ernzerhof, Erratum: Hybrid functionals based on a screened Coulomb potential [J. Chem. Phys. 118, 8207 (2003)], J. Chem. Phys. **124**, 219906 (2006).
[47] F. Ceballos, P. Zereshki, and H. Zhao, Separating electrons and holes by monolayer increments in van der Waals heterostructures, Phys. Rev. Mater. **1**, 044001 (2017).
[48] H. Zeng, G.-B. Liu, J. Dai, Y. Yan, B. Zhu, R. He, L. Xie, S. Xu, X. Chen, W. Yao *et al.*, Optical signature of symmetry variations and spin-valley coupling in atomically thin tungsten dichalcogenides, Sci. Rep. **3**, 1608 (2013).
[49] K. He, N. Kumar, L. Zhao, Z. Wang, K. F. Mak, H. Zhao, and J. Shan, Tightly bound excitons in monolayer WSe_2, Phys. Rev. Lett. **113**, 026803 (2014).
[50] A. Chernikov, T. C. Berkelbach, H. M. Hill, A. Rigosi, Y. Li, B. Aslan, D. R. Reichman, M. S. Hybertsen, and T. F. Heinz, Exciton Binding Energy and Nonhydrogenic Rydberg Series in Monolayer WS_2, Phys. Rev. Lett. **113**, 076802 (2014).
[51] P. Borlido, J. Schmidt, A. W. Huran, F. Tran, M. A. L. Marques, and S. Botti, Exchange-correlation functionals for band gaps of solids: Benchmark, reparametrization and machine learning, npj Comput. Mater. **6**, 96 (2020).
[52] A. Raja, A. Chaves, J. Yu, G. Arefe, H. M. Hill, A. F. Rigosi, T. C. Berkelbach, P. Nagler, C. Schuller, T. Korn *et al.*, Coulomb engineering of the bandgap and excitons in two-dimensional materials, Nat. Commun. **8**, 15251 (2017).
[53] P. Valencia-Acuna, P. Zereshki, M. M. Tavakoli, J.-H. Park, J. Kong, and H. Zhao, Transient absorption of transition metal dichalcogenide monolayers studied by a photodope-pump-probe technique, Phys. Rev. B **102**, 035414 (2020).
[54] F. Ceballos, Q. Cui, M. Z. Bellus, and H. Zhao, Exciton formation in monolayer transition metal dichalcogenides, Nanoscale **8**, 11681 (2016).
[55] Y. Li, A. Chernikov, X. Zhang, A. Rigosi, H. M. Hill, A. M. van der Zande, D. A. Chenet, E.-M. Shih, J. Hone, and T. F. Heinz, Measurement of the optical dielectric function of monolayer transition-metal dichalcogenides: MoS_2, $MoSe_2$, WS_2, and WSe_2, Phys. Rev. B **90**, 205422 (2014).
[56] R. Wang, B. A. Ruzicka, N. Kumar, M. Z. Bellus, H.-Y. Chiu, and H. Zhao, Ultrafast and spatially resolved studies of charge carriers in atomically thin molybdenum disulfide, Phys. Rev. B **86**, 045406 (2012).
[57] Q. Cui, F. Ceballos, N. Kumar, and H. Zhao, Transient absorption microscopy of monolayer and bulk WSe_2, ACS Nano **8**, 2970 (2014).
[58] J. Kunstmann, F. Mooshammer, P. Nagler, A. Chaves, F. Stein, N. Paradiso, G. Plechinger, C. Strunk, C. Schuller, G. Seifert *et al.*, Momentum-space indirect interlayer excitons in transition-metal dichalcogenide van der Waals heterostructures, Nat. Phys. **14**, 801 (2018).
[59] O. Karni, E. Barre, S. C. Lau, R. Gillen, E. Y. Ma, B. Kim, K. Watanabe, T. Taniguchi, J. Maultzsch, K. Barmak *et al.*, Infrared Interlayer Exciton Emission in MoS_2/WSe_2 Heterostructures, Phys. Rev. Lett. **123**, 247402 (2019).

[60] F. Volmer, M. Ersfeld, P. E. F. Junior, L. Waldecker, B. Parashar, L. Rathmann, S. Dubey, I. Cojocariu, V. Feyer, K. Watanabe *et al.*, Twist angle dependent interlayer transfer of valley polarization from excitons to free charge carriers in $WSe_2/MoSe_2$ heterobilayers, arXiv:2211.17210.

[61] E. M. Alexeev, D. A. Ruiz-Tijerina, M. Danovich, M. J. Hamer, D. J. Terry, P. K. Nayak, S. Ahn, S. Pak, J. Lee, J. I. Sohn *et al.*, Resonantly hybridized excitons in moire superlattices in van der Waals heterostructures, Nature (London) **567**, 81 (2019).

[62] C. H. Jin, E. C. Regan, A. M. Yan, M. I. B. Utama, D. Q. Wang, S. H. Zhao, Y. Qin, S. J. Yang, Z. R. Zheng, S. Y. Shi *et al.*, Observation of moire excitons in WSe_2/WS_2 heterostructure superlattices, Nature (London) **567**, 76 (2019).

[63] K. Tran, G. Moody, F. C. Wu, X. B. Lu, J. Choi, K. Kim, A. Rai, D. A. Sanchez, J. M. Quan, A. Singh *et al.*, Evidence for moire excitons in van der Waals heterostructures, Nature (London) **567**, 71 (2019).

[64] Y. Zhu, W.-H. Fang, A. Rubio, R. Long, and O. V. Prezhdo, The twist angle has weak influence on charge separation and strong influence on recombination in the MoS_2/WS_2 bilayer: *Ab initio* quantum dynamics, J. Mater. Chem. A **10**, 8324 (2022).

[65] P. Zereshki, P. Valencia-Acuna, and H. Zhao, All-optical control of charge transfer and interlayer excitons in transition metal dichalcogenide heterostructures, Phys. Rev. B **103**, 165416 (2021).